Computationally Efficient Analysis of Double PM-Rotor Radial-Flux Eddy Current Couplers

Abram S. Erasmus, *Member, IEEE*, and Maarten J. Kamper, *Senior Member, IEEE*

***Abstract*—In this study, a semianalytical calculation method for obtaining 3-D solutions for the torque of radial-flux permanent magnet eddy current couplers is presented. In this way, the use of computationally expensive transient 3-D finite element solutions is avoided, which is very important when it comes to the design optimization of these machines. The proposed analytical method takes the effect of flux density harmonics into account. The 3-D end-effects are taken into account by using Russell's coefficient. The accuracy of the proposed semianalytical calculation method is evaluated against extreme variation of machine dimensions. The Russell end-effect factor is evaluated and found to be inaccurate for axially short and radially large couplers. A prototype coupler with different conductors was tested to validate the proposed semi-analytical torque calculation method.**

***Index Terms*—Analytical analysis, computationally efficient, design optimization, eddy current coupler, radial flux.**

I. Introduction

EDDY CURRENT couplers are popular choices in industrial settings due to efficient operation, vibration isolation, low maintenance, and overload protection, and are commonly used in pump and braking systems. Eddy current couplers can effectively transfer torque between two separate mechanical systems. In these couplers eddy currents are induced in a solid conductor by means of a rotating magnetic field, generating a magnetic reaction field in the conductor and therefore generating torque [1].

Research on permanent magnet (PM) axial-axis eddy current couplers includes amongst others the derivation of functional analytical torque expressions for the coupler [1]–[5]. In this paper, the focus is on an alternative semianalytical method of calculating the torque of a radial-flux eddy current coupler [6]. The proposed semianalytical method includes a 2-D finite element analysis (FEA) static solution, which distinguishes the method fundamentally presented in [2]. The study done by Mouton and Kamper [7] on the design of double PM-rotor radial-axis eddy current couplers has shown to deliver optimum designed prototypes, however, the methodology used for the machine design optimization is found too complex and time consuming.

In the design optimization of radial-flux eddy current couplers, the use of 3-D transient FEA is shown to be necessary for the accurate calculation of the coupler torque [8], [9]. Unfortunately, 3-D transient FEA is computationally expensive in terms of time and computer hardware. A method whereby a 3-D torque solution is obtained from a 2-D calculated torque was developed by Russell for screen-rotor induction motors [10]. By multiplying the 2-D torque result with a coefficient that is proportional to the size and overhang of the model, a 3-D torque result is obtained. Using computational 3-D finite element (FE) analysis Russell's approach has been validated as an effective method to use [11]–[13]. In this paper, a fast semianalytical method is investigated for the accurate calculation of the torque of PM-rotor eddy current couplers at low slip frequencies. First, a 2-D analytical expression for the torque of the coupler is derived and evaluated against 2-D transient FEA. This is then used together with Russell's coefficient to calculate the 3-D torque of the coupler taking end effects into account. The calculated results are verified in the paper by transient 3-D FEA calculations and practical laboratory measurements.

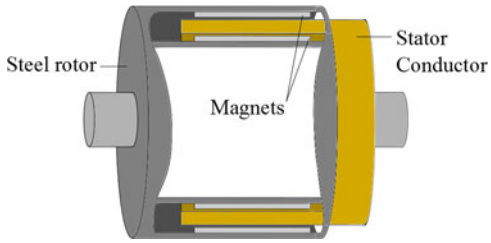

Fig. 1. Radial-flux double PM-rotor eddy current coupler.

II. Eddy Current Coupler for Wind Energy Applications

The radial-flux eddy current coupler shown in Fig. 1 and the real prototype shown in Fig. 2 form the basis of this study.

The coupler consists of two PM rotors mechanically connected to the one shaft of the coupler, and a cylindrical solid conductor (stator) in between the rotors and mechanically connected to the other shaft. The radial axis coupler generates flux in the radial direction by means of the PMs mounted on the surfaces of rotor yokes. The radial-axis coupler has the advantage of less structural (yoke) mass than the axial-axis coupler

Manuscript received November 25, 2016; revised February 24, 2017; accepted March 5, 2017. Date of publication April 4, 2017; date of current version July 15, 2017. Paper 2016-EMC-1216.R1, presented at the 2015 IEEE Energy Conversion Congress and Exposition, Montreal, QC, Canada, Sep. 20–24, and approved for publication in the IEEE Transactions on Industry Applications by the Electric Machines Committee of the IEEE Industry Applications Society. This work was supported by the South African National Research Fund. *(Corresponding author: Abram S. Erasmus.)*

The authors are with the Department of Electrical and Electronic Engineering, Stellenbosch University, Stellenbosch 7599, South Africa (e-mail: aserasmus@sun.ac.za; kamper@sun.ac.za).

Color versions of one or more of the figures in this paper are available online at http://ieeexplore.ieee.org.

Digital Object Identifier 10.1109/TIA.2017.2690986

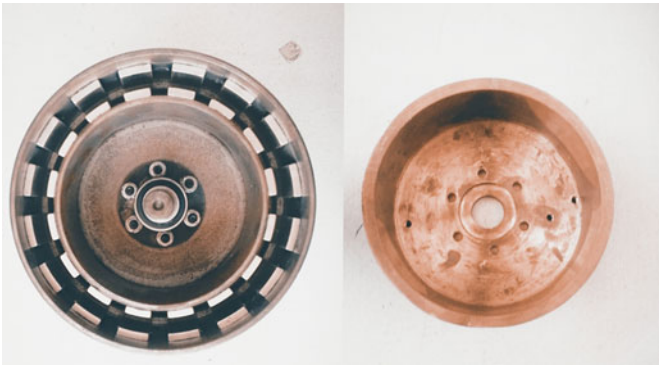

Fig. 2. Double PM rotor and cylindrical copper conductor.

TABLE I
CROSS-SECTIONAL DIMENSIONS OF PROTOTYPE COUPLER

Poles (p)	16	l_{pm}	35 mm
Base Speed	375 r/min	l_{oh}	8.5 mm
θ_m	13.34°	α	0.4857
θ_p	22.5°	β	0.23
l_g	10 mm	h_m	5 mm
h_y	4 mm	h_c	8 mm
r_c	76 mm		

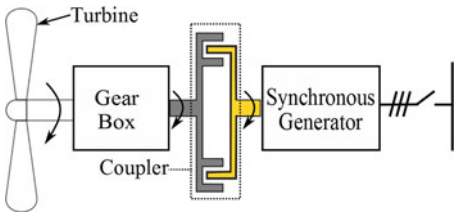

Fig. 3. Eddy current coupler used in wind generator drive system.

to compensate for the strong attraction forces between the two PM rotors. The design specifications of the prototype coupler of Fig. 2 are given in Table I, with explanation of the dimension given in Figs. 4 and 5.

Eddy current couplers are commonly used in pump and braking systems. Another use of these couplers is in wind generator systems, as shown in Fig. 3. Here, the coupler decouples the generator-grid system from the higher frequency torque components of the turbine system. Hence, wind gusts and tower shadowing effects, e.g., are not transmitted to the generator-grid system. The concept is in essence the same as the direct drive concept proposed in [14], where in Fig. 3 the coupler just replaces the slip rotor used in [14]. Together with the mechanical gearbox it is possible to use any standard synchronous generator in the wind energy system.

III. 3-D TORQUE CALCULATION METHODOLOGY

When designing the coupler, 3-D transient FEA calculates the torque which is very close to practical measurements. In this way, the torque of the coupler can be calculated using

$$\tau = \tau_{3\text{D}(\text{FE}t)} \tag{1}$$

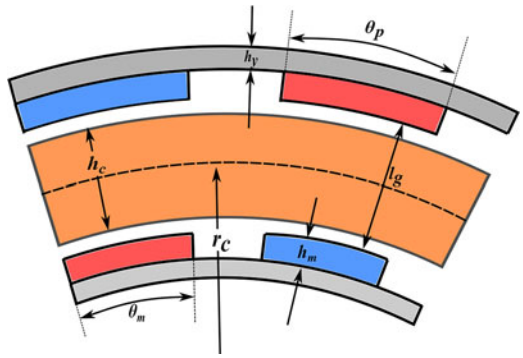

Fig. 4. Radial cross section of the radial-axis eddy current coupler.

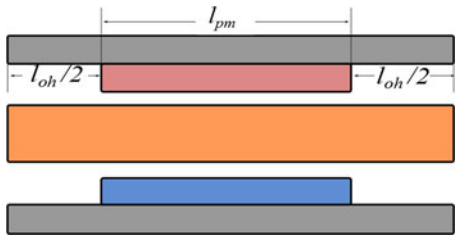

Fig. 5. Axial cross section of the radial-axis eddy current coupler.

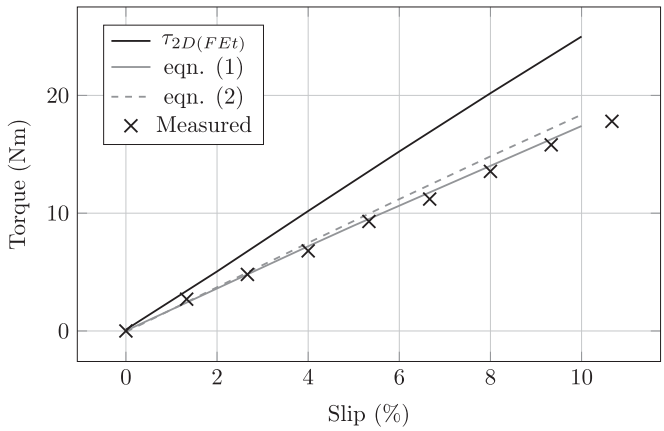

Fig. 6. 3-D FEA (1), semianalytical (2), and measured results of torque versus slip of the prototype coupler.

where $\tau_{3\text{D}(\text{FE}t)}$ is the 3-D transient FE solution of the torque. Although accurate, 3-D transient FE simulations are computationally expensive, and hence completely impractical when used in conjunction with optimization algorithms in the design of the coupler. The 2-D transient FE solution ($\tau_{2\text{D}(\text{FE}t)}$) on the other hand is much faster, but does not deliver correct torque results, as shown in Fig. 6.

In [10], Russell and Norsworthy published a study on eddy currents and wall losses in screen-rotor induction motors, and uses a method of deducing 3-D torque calculations from 2-D results and taking end-effects into account. In this way, the torque of the coupler is calculated as

$$\tau = K_e \tau_{2\text{D}(\text{FE}t)} \tag{2}$$

where $\tau_{2\text{D}(\text{FE}t)}$ is the 2-D transient FE solution of the torque and K_e is the so-called Russell's end-effect factor in [10]. This

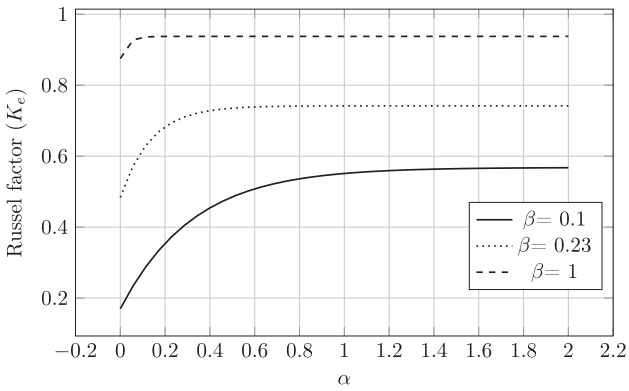

Fig. 7. Russell's end-effect factor as a function of α with β a parameter.

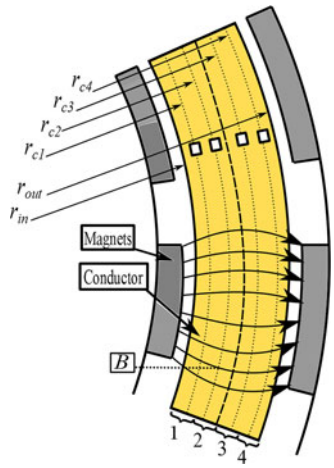

Fig. 8. Cross section of eddy current coupler showing conductor layers.

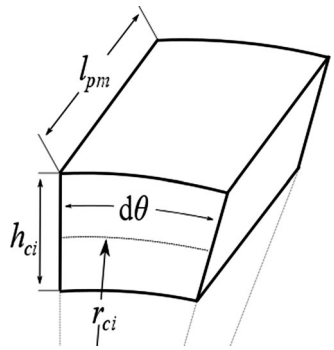

Fig. 9. Element of conductor in the ith conductor layer.

end-effect factor is expressed as

$$K_e = 1 - \frac{\tanh(p\beta)}{(p\beta)(1+\lambda)} \tag{3}$$

where p is the number of poles and $\beta = l_{\text{pm}}/d_c$ with l_{pm} the active axial length of the PM rotors and d_c the center diameter of the cylinder conductor. In (3), λ is the overhang coefficient defined by

$$\lambda = \tanh(p\beta)\tanh(p\alpha\beta) \tag{4}$$

where $\alpha = l_{\text{oh}}/l_{\text{pm}}$ and l_{oh} is the axial overhang length of the cylinder conductor, as shown in Fig. 4. The variation of K_e as a function of α is shown in Fig. 7, with β a parameter.

In a first evaluation of the accuracy of (2), the 2-D transient FE solution shown in Fig. 6 is multiplied by the end factor of the prototype coupler. With $\alpha = 0.4857$ of the prototype coupler, K_e is calculated as $K_e = 0.735$. Using this factor the calculated torque of the coupler according to (2) is as shown in Fig. 6. This shows that an accuracy of within 5% is obtained, which is a first indication that (2) can be used instead of (1) to calculate the torque of the eddy current coupler. Note that in Fig. 6 a slip percentage region of only up to 10% is considered in this study at a base speed of 375 r/min, as given in Table I. This implies a slip frequency region of 0–5 Hz, which is the typical slip frequency region where eddy current couplers operate continuously and where they are optimally designed.

There are, however, two problems with regard to the calculation of the torque by (2). The first is that the 2-D transient FE solution is still too expensive in terms of computational time when used in the design optimization of the coupler. A much faster analytical-based calculation method is required that is proposed and evaluated later in this chapter. The second problem is the accuracy of the Russell factor K_e for extreme design dimensions of the coupler. This is very important when (2) is used in the design optimization of the coupler. In Sections V and VI, the accuracy of K_e is evaluated in detail against 3-D transient FE solutions for radial-flux couplers.

IV. 2-D Torque Calculation Method

This section contains the derivation of an analytical expression for the 2-D torque of the radial-flux coupler, followed by a computationally efficient FEA approach to solve the analytical torque expression.

A. Analytical 2-D Torque Expression

In the proposed analytical calculation of the 2-D torque of the eddy current coupler the solid cylinder conductor is divided into a number of radial layers i, each with an average conductor layer radius r_{ci}, as shown in Fig. 8. Assuming that under low slip frequency the conductor layers are only resistive, and using the Lorentz force law, an expression for the 2-D torque can be derived [6], [10], [15]. Modeling the torque calculated by the current flowing in a conductor element of the cylindrical conductor of the eddy current coupler at electrical position θ, as shown in Fig. 9. The expression for the torque of the element of Fig. 9 in the ith conductor layer is

$$\tau_{\theta i} = \frac{4}{p^2}\frac{r_{ci}^3 h_{ci} l_{\text{pm}}}{\rho}\omega_e B_i(\theta)^2 \mathrm{d}\theta \tag{5}$$

where r_{ci} is the middle radius, h_{ci} the height (thickness), l_{pm} the axial length, and ρ the resistivity of the conductor element. Furthermore in (5), $B_i(\theta)$ is the radial-flux density value and ω_e is the relative electrical angular velocity (or angular slip frequency) between the conductor and the flux density wave. By integrating (5) over one electrical pole pitch of π radians and

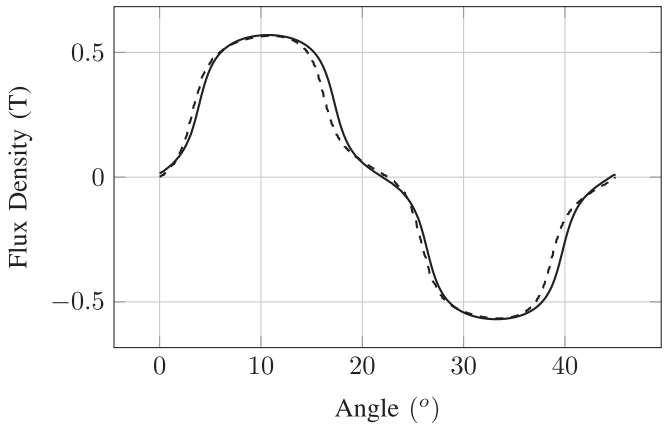

Fig. 10. Radial-flux density waveform of the eddy current coupler with (dotted line) and without(solid line) armature reaction.

multiplying by p poles, the torque of the coupler is given by

$$\tau_{ri} = \frac{4}{p}\frac{r_{ci}^3 h_{ci} l_{\rm pm}}{\rho}\omega_e \int_0^{\pi} B_i(\theta)^2 \mathrm{d}\theta. \quad (6)$$

With $B_i(\theta+\pi) = -B_i(\theta)$ and $B_i(-\theta) = -B_i(\theta)$, there are respectively no even Fourier harmonics and no cosine terms in the series, hence $B_i(\theta)$ of (6) can be expressed as a function of θ as

$$B_i(\theta) = B_{1i}\sin(\theta) + B_{3i}\sin(3\theta) + B_{5i}\sin(5\theta)\ldots. \quad (7)$$

Replacing B_i in (6) by (7) and knowing that for the nth harmonic order that

$$\int_0^{\pi} B_{ni}^2 \sin(n\theta)^2 \mathrm{d}\theta = B_{ni}^2 \frac{\pi}{2} \quad (8)$$

the torque of (6) can be expressed as

$$\tau_{ri} = \frac{2\pi}{p}\frac{r_{ci}^3 h_{ci} l_{\rm pm}}{\rho}\omega_e [B_{1i}^2 + B_{3i}^2 + B_{5i}^2 + \ldots]. \quad (9)$$

In (9), ω_e is the fundamental slip angular frequency. The importance of the layers is that the radial-flux density harmonic content in the layer that is close to the magnets can substantially differ from that in the layers in the middle of the conductor. For thicker conductors, the number of layers is increased to ensure accurate information of the radial-flux density distribution in the conductor. With k layers ($k = 4$ in Fig. 8) the 2-D torque is calculated from (9) simply as

$$\tau_r = \sum_{i=1}^{k} \tau_{ri}. \quad (10)$$

To take the end-effects into account as in (2), the torque of the eddy current coupler is calculated analytically by

$$\tau = K_e \tau_r. \quad (11)$$

B. Semianalytical 2-D Torque Calculation

To consider the effect of armature reaction, Figs. 10 and 11 show the waveforms and flux lines of the radial-flux density in a conductor layer with and without armature reaction; the armature reaction waveform and flux line is obtained from 3-D transient FEA. This shows that the armature reaction effect is small. It was also found that taking this effect into account made very little difference in the torque calculation of (9). Hence, the armature reaction effect on the flux density harmonics is ignored in this calculation method.

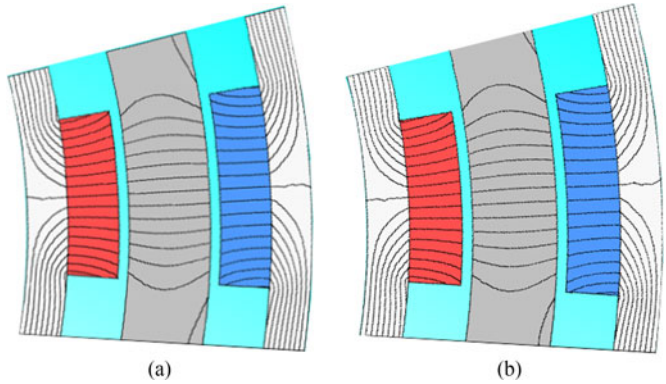

Fig. 11. Flux lines of the radial-flux eddy current coupler with (a) and without (b) armature reaction.

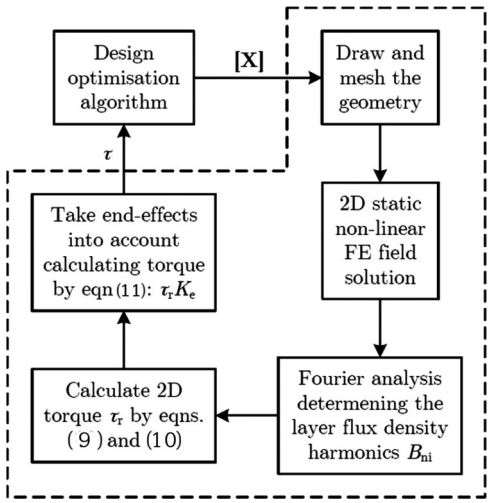

Fig. 12. Torque calculation process in design optimization of the eddy current coupler.

With armature reaction ignored, it is possible to obtain all the radial-flux density harmonic information of all the layers from only one 2-D static nonlinear FE solution and by considering only one pole section of the coupler. Such a solution is very fast and very accurate as it correctly takes into account saturation, curvature-effects and the magnet-material characteristics. The radial-flux density harmonics of (9) of each layer can be obtained by Fourier analysis of the layer radial-flux density waveform available from the 2-D static FE solution. In this study, only the lower flux density harmonic orders of $n = 1, 3, 5, 7$ are considered in (9).

In Fig. 12, the torque calculation method as described above is summarized. Also shown is how this calculation fits in a design optimization process. The optimization algorithm sends the design dimensions and slip frequency of the coupler to the machine analysis software (marked by dotted lines) asking to calculate the torque. The machine analysis software draws and

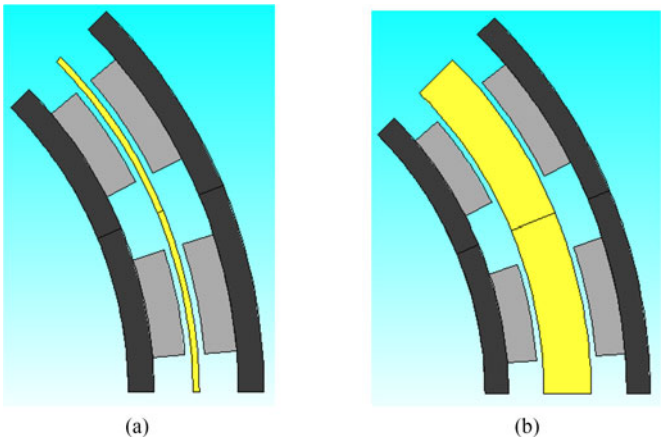

Fig. 13. Radial-flux eddy current coupler with conductor thickness of (a) $h_c = 1$ mm and (b) $h_c = 8$ mm.

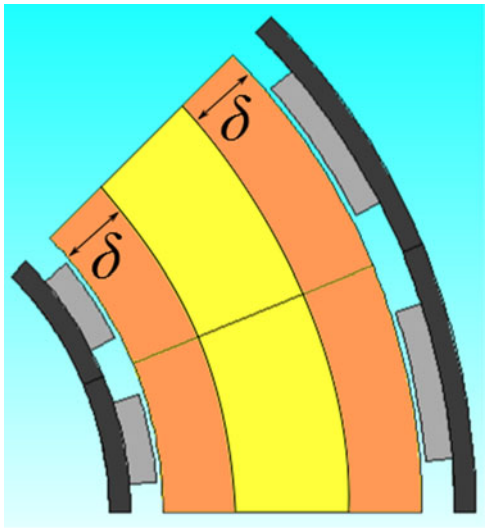

Fig. 14. Radial-flux eddy current coupler with conductor thickness of $h_c = 48$ mm, and δ the skin depth.

meshes the geometry and completes a 2-D static nonlinear FE solution of the given machine structure. From this the Fourier radial-flux density harmonics of the layers are determined, followed by the calculation of the torque according to (9)–(11) and the feedback of the calculated torque τ to the optimization algorithm.

V. 2-D Semianalytical Method Results

It is important in design optimization to confirm the accuracy of the proposed 2-D semianalytical torque calculation of (9) and (10) against 2-D transient FEA torque calculation, $\tau_{2\mathrm{D(FE}t)}$, for extreme variations of machine design dimensions. In this section, the effect of varying the conductor thickness, magnet thickness, and magnet pitch on the accuracy of (9) and (10) is investigated.

A. Conductor Thickness

Three conductor thickness of the prototype coupler are considered in the analyses as shown by the cross sections in Figs. 13 and 14. The torque versus percentage slip results of the different calculations are compared in Fig. 15. It is clear that the results of the semianalytical calculation method are very accurate for conductor thicknesses up to $h_c = 8$ mm and slip speeds up to 5 Hz, as shown in Fig. 15(a). However, when the conductor size is increased to $h_c = 48$ mm, the 2-D transient FE torque of the coupler at high slip speeds is significantly lower than that predicted by (9) and (10), as shown in Fig. 15(b). A more detailed investigation into this calculation error is shown in Fig. 16(a), where the percentage error is plotted versus slip speed with conductor thickness a parameter. From this it is clear that the percentage error in the calculation increases with slip speed and conductor thickness.

The phenomenon in Fig. 16(a) can be explained by the skin effect, which is the tendency of the induced current to flow at higher frequencies only within the skin depth (δ) at the inner and outer surfaces of the cylindrical conductor, as illustrated in

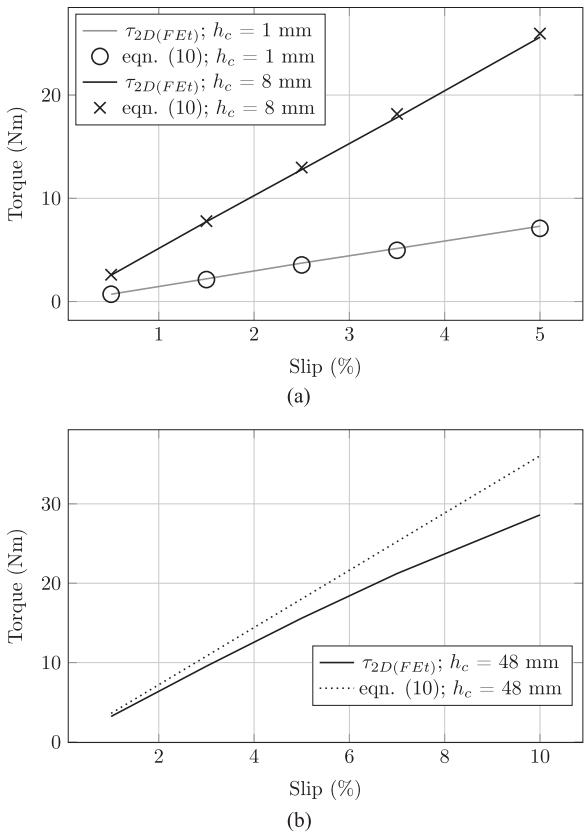

Fig. 15. 2-D analytical and 2-D transient FEA calculated torque versus slip of the eddy current coupler with: (a) $h_c = 1$ mm and $h_c = 8$ mm conductors and (b) $h_c = 48$ mm conductor.

Figs. 14 and 17(a). This skin depth is calculated as follows:

$$\delta = \sqrt{\frac{2\rho}{\omega_e \mu}} \tag{12}$$

where ρ is the resistivity of the conductor, μ the permeability of the conductor, and ω_e the slip frequency. From (12), with an

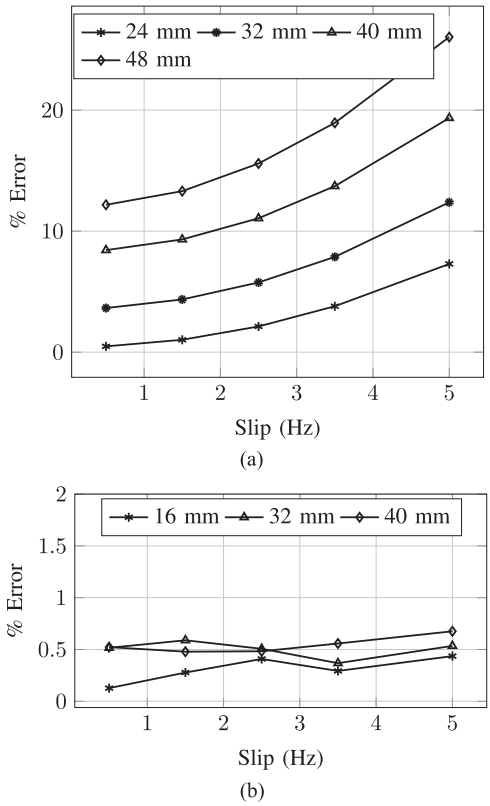

Fig. 16. Percentage error of the 2-D semianalytical torque calculation with conductor thickness a parameter, with skin effect: (a) Not taken into account and (b) taken into account.

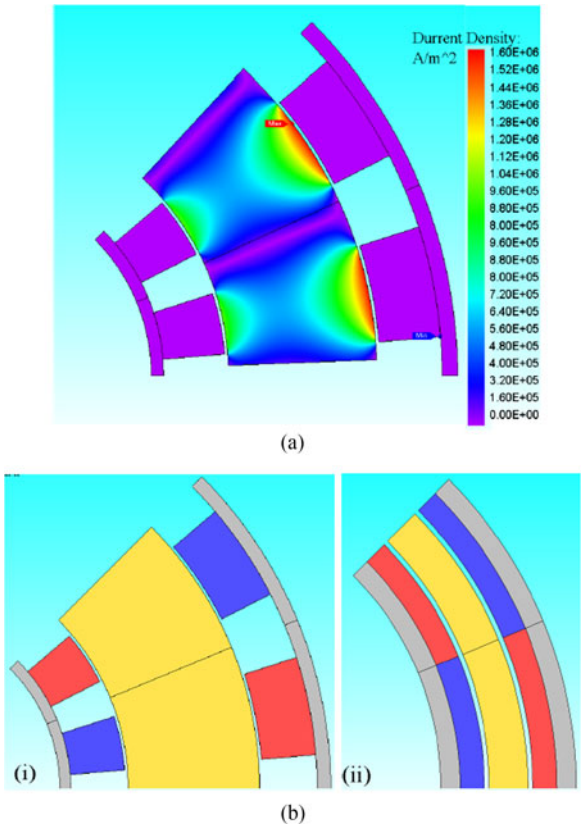

Fig. 17. (a) Visible skin effect where the current density is high only near the inner and outer surfaces of the conductor. (b) Eddy current coupler with thick magnets (left) and magnet pole pitch equal to pole pitch (right).

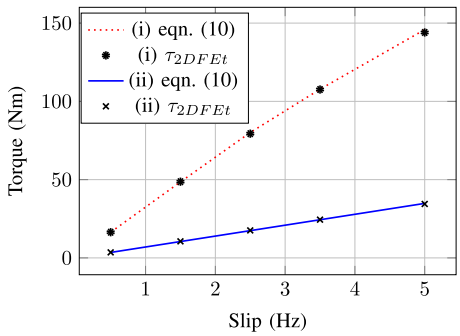

Fig. 18. 2-D semianalytical and transient FEA torque versus slip of the eddy current couplers (i) and (ii) of Figs. 17(b).

increase in slip frequency the skin depth of the induced current flow in the conductor decreases, causing the amount of induced eddy currents and hence torque to reduce, as shown by the results of the 2-D transient FE analysis in Fig. 15(b).

In order to compensate for this in (9), the skin depth δ is first calculated at the considered fundamental slip frequency by (12). If $2\delta < h_c$, then only the layers i that are within the skin depths of the conductor, that is where $r_{\text{in}} < r_{ci} < (r_{\text{in}} + \delta)$ and $(r_{\text{out}} - \delta) < r_{ci} < r_{\text{out}}$, are considered in (9). With skin effect taken into account in this way, the accuracy of the 2-D semianalytical torque calculation of (9) and (10) improves to be within 1% of the 2-D transient FE torque calculation for all conductor thicknesses, as shown in Fig. 16(b). It must be noted that to be strictly correct the skin depths have to be calculated for each harmonic slip frequency $\omega_{en} = n\omega_e$ and then used accordingly to determine the active layers for that harmonic and from that the harmonic torque. This is not used as it was found that it makes very little difference in the calculated torque. The reason for the latter is that with relatively thick conductors the radial-flux density distribution in the conductor is quite sinusoidal with a low harmonic content.

B. Magnet Thickness and Pitch Variation

Two further variations in the dimensions of the prototype eddy current coupler are investigated. In Fig. 17(b)-(i), the magnet thickness is increased, and in Fig. 17(b)-(ii), the magnet pitch is set equal to the pole pitch. The skin effect is shown in Fig. 17(a) for the thick conductor, where the current density remains near the surfaces of the conductor even when the magnet thickness is increased. Taking skin effect now into account in (9) and (10) as described above, the comparisons of torque versus slip of the two calculation methods for both cases of Fig. 17(b) are shown in Fig. 18. This clearly shows the accuracy of the proposed 2-D semianalytical method.

VI. Accuracy of the End-Effect Coefficient

In [16], the accuracy of an analytical equation using K_e of (3) to take end-effects into account is evaluated for axial-flux

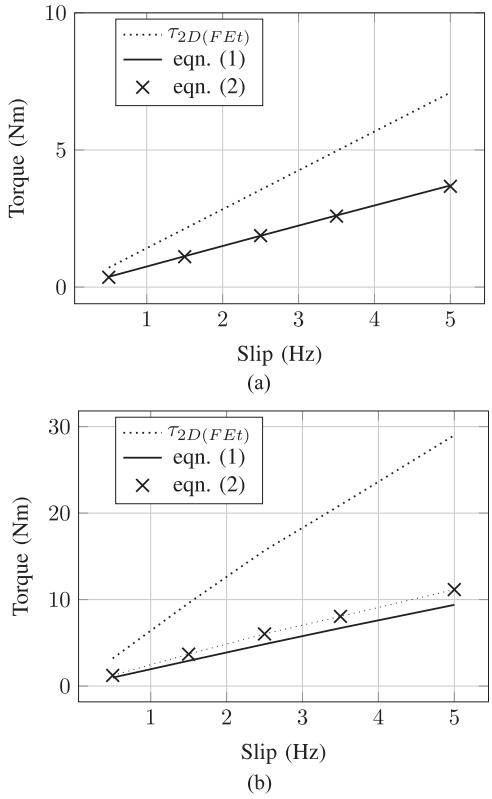

Fig. 19. Accuracy of torque versus slip calculation using Russell's end-effect factor (2), by comparing it with 3-D transient FEA of (1) for: (a) $h_c = 1.0$ mm [$\alpha = 0; \beta = 0.241$]; and (b) $h_c = 48$ mm [$\alpha = 0; \beta = 0.182$].

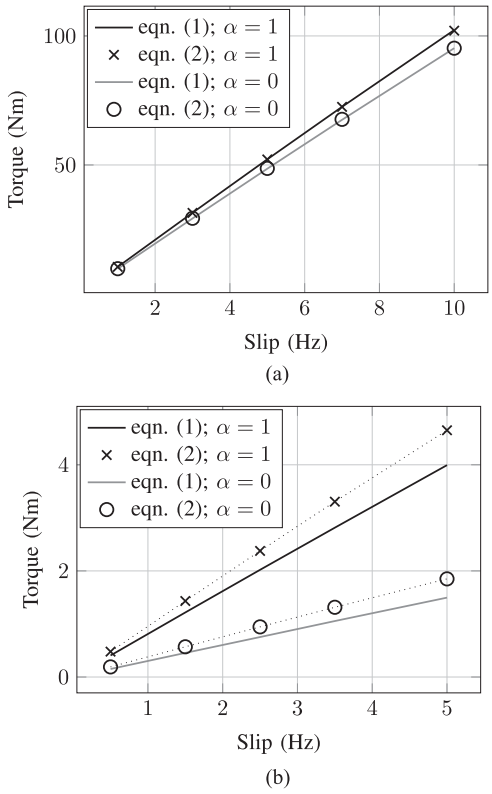

Fig. 20. Comparison of calculated torque versus slip using 3-D transient FEA (1) and Russell's end-effect factor (2) with α a parameter and (a) $\beta = 1$, and (b) $\beta = 0.1$.

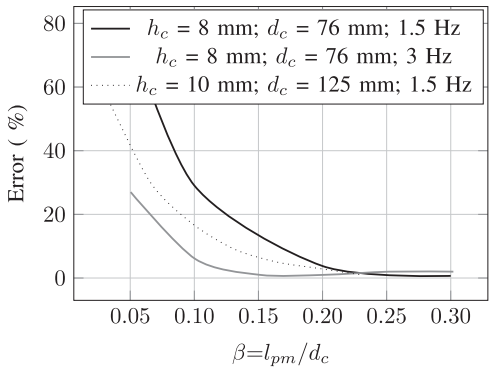

Fig. 21. Percentage calculation error versus $\beta = l_{\text{pm}}/d_c$ with h_c, d_c and frequency parameters.

eddy current couplers with different pole pairs and different conductor dimensions. In this, evaluation errors not larger than 17% were found at a relatively high slip frequency of 12.5 Hz.

In this section, the accuracy of K_e is evaluated for radial-flux eddy current couplers with extreme cylindrical conductor dimensions. The accuracy of K_e is evaluated by comparing the torque calculation of (2) with the 3-D transient FEA calculation as expressed by (1). From (3), it can be seen that K_e is a function of the number of poles and of α and β, as shown in Fig. 7. In this study, the number of poles are kept constant at $p = 16$ as for the prototype, and α and β are varied to the extreme.

In a first comparison the torque versus slip is calculated for thin ($h_c = 1$ mm) and very thick ($h_c = 48$ mm) conductors with $\alpha = 0$ and $\beta = 0.241$ (thin conductor) and $\beta = 0.182$ (thick conductor). The results of this calculation, as shown in Fig. 19, show excellent comparison with $\beta = 0.241$, but with about a 16% error when $\beta = 0.182$.

In Fig. 20, the calculated torque versus slip results are shown for $\alpha = 0$ and $\alpha = 1$ and with $\beta = 0.1$ and $\beta = 1.0$. Note that Fig. 6 shows the results for the prototype with $\beta = 0.23$. There is very good agreement between the results of (1) and (2), except for the cases where β becomes small (i.e., axially short, radially large couplers), as in Figs. 19(b) and 20(b).

To investigate the error in the calculation in more detail when beta becomes small, the eddy current coupler of Fig. 13(b) was simulated at slip frequencies of 1.5 and 3 Hz for small to large values of beta. This simulation study was also repeated for a larger in diameter coupler. The results of the percentage error found in the calculation compared to 3-D FEA results are shown in Fig. 21. It is clear that with $\beta < 0.2$ the accuracy of the end-effect coefficient K_e of (3) drops, with errors in the calculated torque according to (2) larger than 10%.

VII. Practical Results and Method Validation

The measurement setup for the practical tests is shown in Fig. 22(a), where the torque and slip frequency of the coupler are measured [15]. Four conductor rotors, as shown in Fig. 22(b), were tested; the design detail of the conductor rotors is summarized in Table II. For the torque calculations of the coupler with

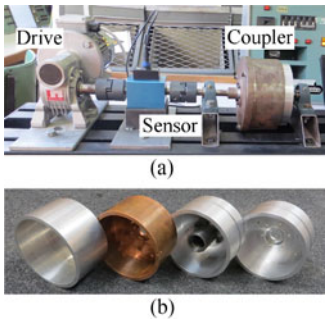

Fig. 22. Eddy current coupler prototype: (a) Practical laboratory test set up; and (b) four conductor types explained in Table II.

TABLE II
CONDUCTOR PROPERTIES

Conductor	1	2	3	4
Material	Cu	Al	Al	Al
h_c	8 mm	8 mm	8 mm	8 mm
l_{oh}	Max	Max	Equal	Zero
τ at 2 Hz	6.8 Nm	3.35 Nm	3.4 Nm	2.6 Nm
α	0.243	0.243	0.143	0

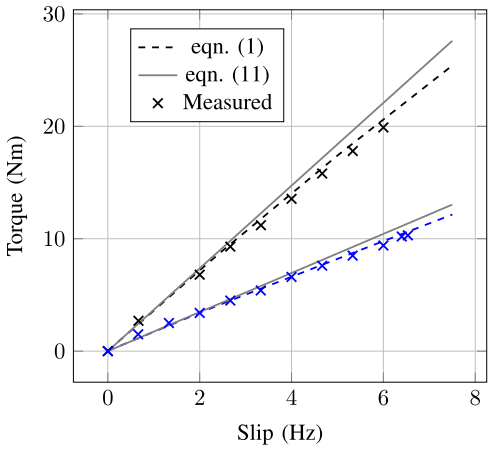

Fig. 23. Torque versus slip frequency of copper (top graph) and aluminum (bottom graph) conductors 1 and 2 of Table II.

the different conductors, (1) and (11) were used. The torque calculations were done at the same conductor temperatures as were measured. The built models were run and tested under rated conditions to verify the temperature range of the coupler. A temperature of 60 °C was measured after 60 min of the operation time.

The calculated and measured results of the coupler with the four conductors are shown in Figs. 23 and 24. From this it is clear that the calculated results according to (1) and (11) correlate well with each other and also compare well with the measured results. Furthermore, the huge effect of copper conductor material above aluminum on the torque performance of the coupler is clear from Fig. 23; the torque almost doubles with copper material due to the much lower resistivity of copper. Finally, the effect of conductor overhang on the torque performance of the coupler, which is shown in Fig. 24, where the

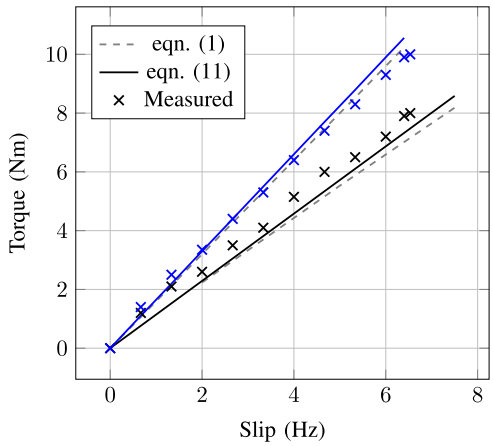

Fig. 24. Torque versus slip frequency of the equal (top graph) and zero (bottom graph) overhang aluminum conductors 3 and 4 of Table II.

overhang conductor generates a larger torque as also predicted by the Russell factor.

VIII. CONCLUSION

In this paper, a fast and accurate semianalytic torque calculation method for double PM-rotor eddy current couplers is proposed and evaluated. The results are compared to a built prototype with various conductor types. The following main conclusions are drawn from the results.

1) The proposed 2-D torque calculation method that requires one static FE solution is found to be very accurate at low slip frequency values for extreme variations of machine dimensions. The method takes yoke saturation, curvature-effects, magnet-characteristics, skin effect, and radial air gap flux density harmonics into account in the torque calculation. This distinguishes the method from other analytical methods.
2) It is shown that the Russell factor becomes less accurate when used to account for 3-D end-effects if $\beta < 0.2$, i.e., for radial-flux couplers that are axially short and radially large. However, for designs with $\beta > 0.2$, which is typically the case, calculation accuracies of within 5% of 3-D transient FEA calculations are found. This makes the use of the proposed semianalytic calculation method very attractive in the design optimization of the coupler.
3) The Russell end-effect factor is evaluated in terms of zero and equal overhang conductors. It is shown that the 3-D end effect factor is accurate for zero and equal conductor overhangs. These results suggest that there is an optimum overhang, where torque per conductor material cost becomes a maximum.
4) It is shown that the proposed semianalytical method predicts the torque of the coupler very accurately compared to measured results for various conductor materials and conductor overhangs. In these calculations and measurements, amongst others, the almost doubling effect on the torque performance of the coupler with copper material above aluminum material is shown.

ACKNOWLEDGMENT

The authors would like to thank the South African National Research Fund for their continued financial support, and to C.H.O Lombard for his contribution to this paper with regard to the measurements.

REFERENCES

[1] A. Canova and B. Vusini, "Analytical modeling and analysis of axial-flux interior permanent-magnet couplings," *IEEE Trans. Magn.*, vol. 61, no. 11, pp. 5940–5947, 2014.

[2] T. Lubin, S. Mezani, and A. Rezzoug, "Simple analytical expressions for the force and torque of axial magnetic couplings," *IEEE Trans. Energy Convers.*, vol. 27, no. 2, pp. 536–546, Jun. 2012.

[3] S. Mohammadi, M. Mirsalim, and S. Vaez-Zadeh, "Nonlinear modeling of eddy-current couplers," *IEEE Trans. Energy Convers.*, vol. 29, no. 1, pp. 224–231, Mar. 2014.

[4] J. Wang, H. Lin, S. Fang, and Y. Huang, "A general analytical model of permanent magnet eddy current couplings," *IEEE Trans. Magn.*, vol. 50, no. 1, Jan. 2014.

[5] S. Mohammadi, M. Mirsalim, S. Vaez-Zadeh, and H. A. Talebi, "Analytical modeling and analysis of axial-flux interior permanent-magnet couplers," *IEEE Trans. Ind. Electron.*, vol. 61, no. 11, pp. 5940–5947, Nov. 2014.

[6] A. S. Erasmus and M. J. Kamper, "Analysis for design optimisation of double PM-rotor radial flux eddy current couplers," in *Proc. 2015 IEEE Energy Convers. Congr. Expo.*, Sep. 2015, pp. 6503–6510.

[7] Z. Mouton and M. J. Kamper, "Design of an eddy-current coupling for slip-synchronous permanent magnet wind generators," in *Proc. 2012 20th Int. Conf. Elect. Mach.*, 2012, pp. 633–639.

[8] S. Mohammadia and M. Mirsalim, "Design optimization of double-sided permanent-magnet radial-flux eddy-current couplers," *Elect. Power Syst. Res.*, vol. 108, pp. 282–292, 2013.

[9] S. Mohammadi and M. Mirsalim, "Double-sided permanent-magnet radial-flux eddycurrent couplers: Three-dimensional analytical modelling, static and transient study, and sensitivity analysis," *IET Elect. Power Appl.*, vol. 7, no. 9, pp. 665–679, Nov. 2013.

[10] R. Russell and K. Norsworthy, "Eddy currents and wall losses in screened-rotor induction motors," *Proc. IEE—Part A, Power Eng.*, vol. 105, no. 20, pp. 163–175, Apr. 1958.

[11] K. Yamazaki *et al.*, "Reduction of magnet eddy-current loss in interior permanent-magnet motors with concentrated windings," *IEEE Trans. Ind. Appl.*, vol. 46, no. 6, pp. 2434–2441, Nov./Dec. 2010.

[12] J. D. Edwards, B. V. Jayawant, W. R. C. Dawson, and D. T. Wright, "Permanent-magnet linear eddy-current brake with a non-magnetic reaction plate," *IEEE Proc.—Elect. Power Appl.*, vol. 146, no. 6, pp. 627–631, Nov. 1999.

[13] K. Yamazaki, "Modification of 2D nonlinear time-stepping analysis by limited 3D analysis for induction machines," *IEEE Trans. Magn.*, vol. 33, no. 2, pp. 1694–1697, Mar. 1997.

[14] J. Potgieter and M. Kamper, "Design of new concept direct grid-connected wind generator," *IEEE Trans. Ind. Appl.*, vol. 48, no. 3, pp. 913–922, May/Jun. 2012.

[15] C. H. O. Lombard and M. J. Kamper, "Theoretical and finite element analysis of a double rotor radial flux permanent magnet eddy current coupling," in *Proc. Southern Afr. Univ. Power Eng. Conf.,* Johannesburg, South Africa, Jan. 2015.

[16] T. Lubin and A. Rezzoug, "Steady-state and transient performance of axial-field eddy-current coupling," *IEEE Trans. Ind. Appl.*, vol. 62, no. 4, pp. 2287–2296, Apr. 2015.

Abram S. Erasmus (M'16) received the B.Eng. and M.Sc. degrees (electrical engineering) in electrical machine design and design optimization from Stellenbosch University, Stellenbosch, South Africa, in 2015 and 2016, respectively.

His research interests include electrical machine design, design optimization, wind turbine drivetrains, and energy efficiency.

Maarten J. Kamper (SM'08) received the M.Sc. and Ph.D. degrees in engineering from the University of Stellenbosch, Stellenbosch, South Africa, in 1987 and 1996, respectively.

Since 1989, he has been a member of the academic staff with the Department of Electrical and Electronic Engineering, University of Stellenbosch, where he is currently a Professor of electrical machines and drives.

Prof. Kamper is also a South African National research Foundation Supported Scientist and a registered Professional Engineer in South Africa. His research interests include computer-aided design and control of reluctance permanent magnet, and induction machine drives.